ROLE OF PARTICLES OF THE TARGET MATERIAL IN THE DYNAMICS OF AN EROSIVE JET FORMED BY A LASER BEAM

V. K. Goncharov

UDC 621.373.826:533.9

Empirical substantiation is offered for a model of the destruction of metal by moderate-intensity (10^5-10^8 W/cm^2) laser radiation. The model allows for the presence of a finely dispersed liquid-droplet phase of the target material in the erosive jet. This phase is formed by the mechanism of bulk vaporization.

In the action of laser radiation of moderate intensity (10^5-10^8 W/cm^2) on metals, the resulting products of the metal's disintegration propagate counter to the laser beam. In this case, the laser radiation incident on the target interacts not only with the surface, but also with the disintegration products. These products may have an effect on the passage of the laser radiation to the target surface [1-10]. Questions related to the transport of the energy of laser radiation through an erosive jet to the surface of a target are very important both from the viewpoint of optimizing regimes for the laser treatment of materials and in regard to calculation of the plasmodynamic pattern that results from the action of moderate-intensity laser radiation on different materials.

To study the effect of erosion products on the propagation of laser radiation, an experiment was set up in [11] to measure the radiant-energy balance from an auxiliary laser which probed the erosive jet formed by radiation from another, more powerful laser. The experimental scheme is depicted in Fig. 1. Radiation from a neodymium laser in the free-generation regime was focused on a zinc target placed at the center of the integrating sphere. The total energy of the radiation ranged up to 1.5 kJ, with a pulse duration of 10^{-3} sec. The radiation from the neodymium laser was focused by a lens with a focal distance of 25 cm to a spot 7.5 mm in diameter. The power of the radiation was measured with the use of neutral light filters. The erosive jet that was formed was probed by radiation from a auxiliary ruby laser operated in the regular-pinch regime. Total generation time for the ruby laser was $1.5\text{-}10^{-3}$ sec. The diameter of its light beam was varied within the range 1.5-2 mm. The erosive jet was probed at a distance of 1.5 mm from the surface of the target. The power density of the radiation from the ruby laser was no greater than 10^4 W/cm^2 – so as not to perturb the parameters of the medium being probed. The energies of the radiation from both lasers were monitored with IKT-1N calorimeters. The time characteristics of the neodymium laser were checked by means of a photocell 14 (Fig. 1). The power of the probing radiation $P_{inc}(t)$ of the ruby laser incident on the erosive jet was measured with photocell 21, while the power of the transmitted radiation $P_{tr}(t)$ was measured with photocell 27. The power of the radiation of the ruby laser scattered by the erosive jet $P_{sca}(t)$ was determined with photocell 24. The signals from the photocells were sent to recording oscillographs S8-2. As the photocells, we used FD-9 photodiodes in all of the channels except the scattering channel. Here, we used an FÉU-68 photodiode to obtain maximum sensitivity. All of the measuring devices were calibrated before the experiments. Glass light filters 13, 20, 22 and 25 were placed in front of the photocells to eliminate the effect of background illumination. However, this proved insufficient for the photocells which recorded the transmitted and scattered radiation. To eliminate the interfering effect of the radiation from the erosive jet and the neodymium laser, we additionally placed interference light filters 23 and 26 in front of these photocells. The filters corresponded to the wavelength of the radiation from the ruby laser.

Thus, we simultaneously recorded the power of the incident, transmitted, and scattered radiation of the ruby (probe) laser in the experiment. It is obvious that for the probing radiation

$$P_{inc}(t) = P_{tr}(t) + P_{sca}(t) + P_{abs}(t), \tag{1}$$

A. N. Sevchenko Scientific-Research Institute of Applied Physics Problems, Minsk. Translated from Inzhenerno-Fizicheskii Zhurnal, Vol. 62, No. 5, pp. 665-684, May, 1992. Original article submitted November 12, 1991.

1062-0125/92/6205-0472$12.50

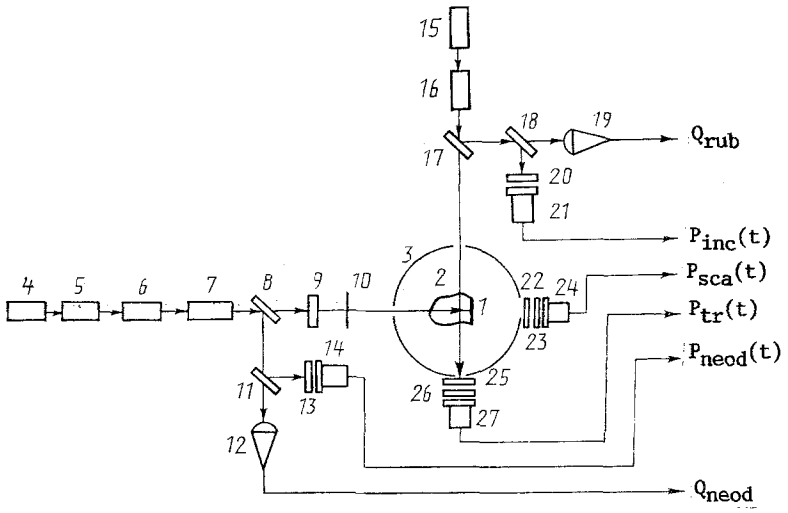

Fig. 1. Setup of the experiment: 1) target; 2) erosive jet; 3) integrating sphere; 4, 15) helium–neon control lasers; 5) neodymium laser; 6, 7) amplifiers; 8, 11, 17, 18) beam splitters; 9, 13, 20, 22, 25) glass light filters; 10) focusing lens; 12, 19) energy meters; 14, 21, 24, 27) photodetectors; 16) probing ruby laser; 23, 26) interference light filters.

i.e. the power of the ruby-laser radiation incident on the erosive jet was equal to the sum of the powers of the radiation transmitted, scattered, and absorbed by the erosive jet. Normalizing with respect to unity, we obtain

$$K_{tr}(t) + K_{sca}(t) + K_{abs}(t) = 1, \tag{2}$$

where

$$K_{tr}(t) = \frac{P_{tr}(t)}{P_{inc}(t)}; \quad K_{sca}(t) = \frac{P_{sca}(t)}{P_{inc}(t)}; \quad K_{abs}(t) = \frac{P_{abs}(t)}{P_{int}(t)}.$$

Thus, by measuring $P_{inc}(t)$, $P_{tr}(t)$, and $P_{sca}(t)$, we can find the transmission and scattering coefficients of the probe radiation and thus calculate the absorption coefficient from (2). Curves of $K_{tr}(t)$, $K_{sca}(t)$, and $K_{abs}(t)$ are shown in Fig. 2.

In all of the experiments, we reckoned time beginning with the initial action of the radiation from the neodymium laser.

Simultaneous with the probing of the erosive jet by radiation from the ruby laser, we made spectroscopic measurements of temperature and electron concentration in the plasma of the jet. These quantities were determined by comparing the measured and theoretically calculated emissivities of the plasma and the ratios of these values for two spectral ranges. The emissivities were measured with a photographic recording unit (HSR-1) acting as a high-speed, slow-motion camera. The unit was equipped with a double lens insert. Two interference filters with transmission maxima at 432 and 686 nm and half-widths of 5 and 17 nm, respectively, were placed on the inlet diaphragm of the unit. Preliminary spectral studies of the plasma showed the absence of spectral lines in the transmission-band range of the interference filters. The inlet diaphragm was changed so that images of the plasma at difference wavelengths were recorded simultaneously. The image of the plasma jet was focused on the film of the SFR-1 so that the jet axis was perpendicular to the optical axis of the SFR-1. The velocity of the mirror of the SFR-1 was 7500 rpm. Exposure per frame was 16 μsec.

Thus, two images of the plasma jet in two wavelength ranges were obtained on the SFR-film. To obtain absolute values of the emissivities of the plasma at the indicated wavelengths, we photographed chronograms of the radiation from an ISP-5000 flash lamp under the same conditions. The flash lamp acted through a nine-stage attenuator. Before the recording, the radiation from this lamp was calibrated using a standard ÉV-45 light source. Such measurements allowed us to determine the beam-averaged emissivity of the plasma for two spectral ranges with time and space resolution.

We theoretically calculated emission in the continuous spectrum for the presumed parameters of the plasma, assuming that the emission was due to recombination and deceleration of electrons. The overall coefficient for recombination emission was determined by summation of the values for individual quantum levels. Here, we assumed the existence of equilibrium distributions of the electrons with respect to velocity and of the ions with respect to energy level – in accordance with the method described in [12]. Recombination at levels with the orbital quantum number $l < 3$ was calculated by the quantum-defect method

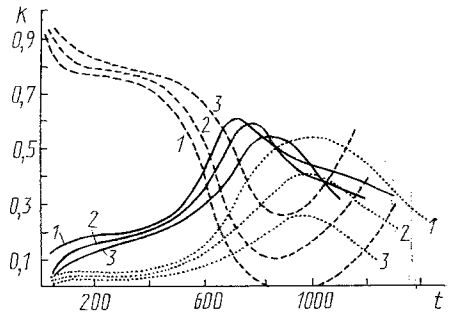

Fig. 2. Change in the transmission (dashed curves), scattering (dotted curves), and absorption (solid curves) coefficients over time with a neodymium-laser energy of 1300 (1), 900 (2), and 340 J (3). t, μsec.

[13], while recombination at levels $l \geq 3$ was calculated from the formula for hydrogenlike atoms with allowance for the Gant formula [14]. The decrease in ionization potential was accounted for by means of the English–Teller [15] formula. Bremsstrahlung intensity in the ion field was calculated in a quasiclassical approximation with the Gant correction given by the analytical expression presented in [16]. The continuum created by deceleration of electrons on atoms was calculated in terms of the corresponding elastic scattering cross section with the use of the theoretical formula in [17].

Figure 3 shows the results of spectroscopic measurements at the probing height in the axial zone of the erosive jet. Figure 4 shows the path of plasma temperature and electron concentration over the radius of the jet at the probing height. The paths of the curves $K_{tr}(t)$, $K_{sca}(t)$, and $K_{abs}(t)$ cannot be attributed to the main processes associated with the absorption of radiation by the plasma because such absorption is negligible for the given plasma parameters. To estimate absorption of the probe radiation (λ = 693 nm) by the plasma, we performed a calculation similar to the calculations of emissivity. Since the energy of a quantum of the probe radiation was small compared to the ionization potential in our case, the results were similar to those obtained from the approximate Kramers–Unsold formula [18].

The overall absorption coefficient for the experiment with 340 J as the energy of the radiation of the plasma-forming laser was less than 0.002, while a value of 0.03 was obtained for an energy of 900 J. Even for the maximum parameters of the plasma jet (see Fig. 3), absorption in the plasma did not exceed 0.09 and was considerably less than the experimental value.

Rayleigh and Thomson scattering also cannot explain the path of the curve $K_{sca}(t)$, since their cross sections are estimated as $1.8 \cdot 10^{-26}$ and $0.67 \cdot 10^{-24}$ cm^2 in our case [19]. To determine the role of turbulent regions in the plasma as scattering centers for the probe radiation, we recorded time-lapse interferograms of the plasma jet at the wavelength of the ruby-laser radiation. Correlation analysis of the interferograms by the method described in [20] allowed us to determine the characteristic integral turbulence scale of the plasma. In our case, this turned out to be equal to 3-5 mm. We also estimated the effect of deflections of the probing beam due to nonuniformity of the refractive index in the plasma. These estimates, made by the method described in [21], showed that refraction had no effect on the probe beam even for discontinuities in the plasma of the dimensions ~0.1 mm (within this range, electron concentration varies within the range 10^{17}-10^{18} cm^{-3}.

The most likely mechanism determining $K_{tr}(t)$, $K_{sca}(t)$, and $K_{abs}(t)$ is absorption and scattering of the radiation from the ruby probe laser on particles of a liquid-droplet phase of the target material. The path of the curves of $K_{tr}(t)$, $K_{sca}(t)$, and $K_{abs}(t)$ shows (see Fig. 2) that $K_{tr}(t)$ decreases but $K_{sca}(t)$ and $K_{abs}(t)$ increase during the first 50 μsec, reaching steady-state values. There is little change during the next 500 μsec. Within the period 500-600 μsec, after the beginning of action of the radiation, the coefficients change sharply – depending on the energy of the neodymium-laser radiation – and they reach extreme values by the end of the radiation pulse (800-900 μsec). Such sharp changes in the coefficients can be attributed to the appearance of a large number of liquid droplets of the target material by the end of the laser pulse. These droplets appear because a crater is formed in the region affected by the laser radiation over time, this crater being the result not only of vaporization but also several secondary processes: heating of the walls formed inside the crater by vapors and scattered radiation, followed by their fusion and hydrodynamic erosion by the outgoing gas flow [22]. By the end of the laser radiation, the pressure pulse generated in the crater ejects the liquid phase from the crater in the form of relatively coarse drops [23].

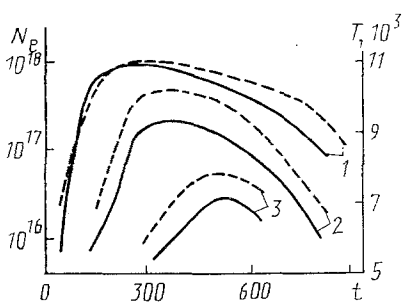

Fig. 3

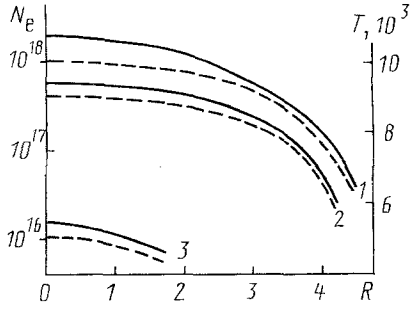

Fig. 4

Fig. 3. Change in the concentration of electrons (dashed curves) and plasma temperature (solid curves) over time for a neodymium-laser energy of 1300 (1), 900 (2), and 340 J (3). N_e, cm^{-3}, T, K.

Fig. 4. Radial change in plasma temperature (solid curves) and electron concentration (dashed curves) with a neodymium-laser energy of 1300 (1), 900 (2), and 340 J (3). R, mm.

However, absorption and scattering of the probe radiation by the erosive jet occurs over the entire period of action of the neodymium-laser radiation (see Fig. 2) – it just occurring to a lesser degree than at the end of the pulse. Such absorption and scattering can be attributed to the appearance of target-material particles at the very beginning of plasma formation as a result of explosive vaporization (bulk vaporization) [1, 4, 24]. This occurs because the formation of particles as a result of hydrodynamic erosion of the crater walls (particularly during the initial action) is made difficult by the shallowness of the crater. Even after the laser radiation has acted, crater depth is no greater than 0.3 mm, while its diameter is 7.5 mm.

Although bulk vaporization in a thin absorption layer is difficult at power densities 10^6-10^8 W/cm^2 for metals not containing impurities or structural defects [25], this phenomenon can be realized as a result of the spatial nonuniformity of laser-radiation power density characteristic of generation in the free regime. Bulk vaporization is facilitated appreciably by the presence of dissolved gases in the metal [26, 27].

An experiment conducted with a self-generating impulsive optical discharge [28] offers convincing proof that laser radiation is lost as a result of absorption and scattering on particles of a liquid-droplet phase. Such a discharge is obtained by focusing laser radiation on the target if the focus of the lens is located several centimeters from the target surface. In this case, laser-radiation power density on the target is always lower than in front of it, and it reaches its maximum value in the region of the caustic of the lens. The target erosion products, moving counter to the laser beam, interact with radiation of ever-increasing power density. An optical discharge is initiated in the region of the caustic of the lens at a certain value of laser power. An experiment was conducted with a zinc target and focusing of the radiation from a neodymium laser with an energy of 1 kJ and a duration of $\sim 10^{-3}$ sec. The focal distance of the lens was 22.5 cm. The focus of the lens was located 4 cm from the target surface. Power density was 10^6 W/cm^2 on the target surface and 10^7 W/cm^2 in the focal region. The experiment involved transverse probing of the optical discharge by radiation from a ruby laser at different distances h from the target surface and determination of the attentuation factor $K_{at}(t) = 1 - K_{tr}(t)$. As the experiments showed [28], the attentuation factors at different heights change little within the time interval 150-500 μsec. Thus, the moment $t^* = 300$ μsec was chosen and a graph of steady-state values of the attenuation factor of the probe radiation was constructed for this moment as a function of h (Fig. 5).

Simultaneous with probing of the self-igniting optical discharge, spectroscopic methods were used to measure electron concentration N_e and plasma temperature T along the axis of the discharge. As shown by Fig. 5, plasma temperature is negligible near the target and amounts to $\sim 4.5 \cdot 10^3$ K. After decreasing with increasing distance from the target, it remains constant. With the transition to the focus of the lens, plasma temperature increases sharply to $12 \cdot 10^3$ K. Electron concentration behaves similarly, increasing from $\sim 10^{16}$ cm^{-3} near the target to $5 \cdot 10^{17}$ cm^{-3} in the focal region. High-speed filming showed that an optical discharge is initiated in the region where temperature and electron concentration increase sharply. The generation of the discharge is evident from the presence of the highly luminous region with sharp boundaries. However, the attenuation factor expressing attenuation of the probe radiation by the erosive jet is maximal near the target surface and decreases sharply with increasing distance from it. It changes little at distances greater than 1 cm. An analysis of the curves in Fig. 5 shows that the region in which attenuation of the laser radiation is maximal is located near the target – where the liquid-droplet phase is

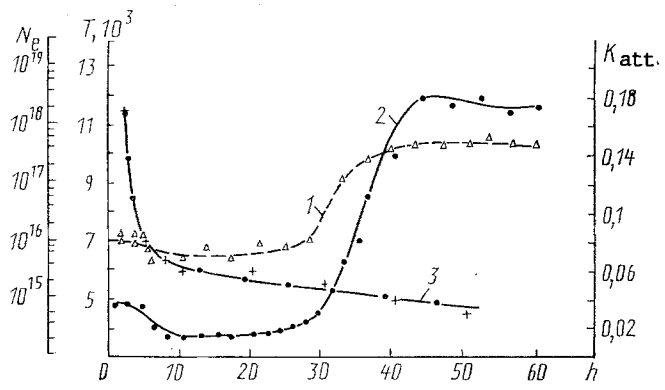

Fig. 5. Change of electron concentration N_e (1), temperature T (2), and steady-state values of the attenuation factor K_{as} (3) along the optical discharge for a zinc target. h, mm; T, K.

found – rather than in the region where the parameters of the plasma are maximal, i.e. in the focal region. Thus, the losses of laser radiation are determined for the most part not by the main loss mechanisms in the plasma, but by absorption and scattering of the liquid-droplet phase of the target material.

The relationship between $K_{abs}(t)$ and $K_{sca}(t)$ should change in relation to the dimensions of the target-material particles. The following relations [29] have been established for small ($d << \lambda$) particles

$$Q_s = \frac{8}{3}\pi^4\left(\frac{d}{\lambda}\right)^4\left|\frac{m^2-1}{m^2+2}\right|^2, \quad Q_b = -4\pi\frac{d}{\lambda}\,\mathrm{Im}\left(\frac{m^2-1}{m^2+2}\right),$$

where d is particle diameter; λ is the wavelength of the probe radiation; Q_s and Q_a are dimensionless scattering and absorption coefficients referred to the cross-sectional area of a particle. The complex refractive index m is connected with the refractive index n and absorption index χ by the relation $m = n - i\chi$. Considering that

$$|m^2-1|^2 = (n^2-\chi^2-1)^2+4n^2\chi^2, \quad \mathrm{Im}\left(\frac{m^2-1}{m^2+2}\right) = \frac{-6n\chi}{|m^2+2|^2},$$

we obtain:

$$\frac{Q_s}{Q_b} = \frac{\pi^3}{9}\left(\frac{d}{\lambda}\right)^3\frac{(n^2-\chi^2-1)^2+4n^2\chi^2}{n\chi}. \tag{3}$$

It is evident from Eq. (3) that a decrease in particle dimensions is accompanied by a decrease in radiation scattering losses compared to absorption, while absorption – if it exists becomes the principal factor for very small particles.

For large particles ($d >> \lambda$), the relationship between scattering and absorption depends only on the physical nature of the substance of the particles. It can be evaluated [30] from the formula

$$\frac{Q_s}{Q_b} = \frac{n^2+n+\chi^2+(1+n)^2+2\chi^2}{2n[(1+n)^2+\chi^2]}. \tag{4}$$

It can be seen from Eq. (4) that $Q_s > Q_a$ for the metallic particles investigated here in the case of probe radiation of the wavelength 0.7 μm. Passing to the limit of very large particles, we obtain the reflection and absorption coefficients of a massive target – for which reflection might be an order of magnitude or more greater than absorption.

Thus, the relationship between the scattering and absorption coefficients can be used to qualitatively evaluate characteristic particle dimensions. It is evident from Fig. 2 that small particles, i.e. particles of a diameter much less than the wavelength of the probe radiation, are formed near the target surface at the beginning of the radiation pulse from the neodymium laser. By the end of the pulse, it is apparent from the ratio of the scattering and absorption coefficients that coarse particles have entered

the erosive jet, i.e. particles of a diameter much greater than the wavelength of the probe radiation from the ruby laser. As already indicated, the appearance of relatively coarse particles of the target material in the form of liquid drops by the end of the pulse is attributable to the action of the hydrodynamic mechanism [22, 23]. The most likely mechanism of formation of the finely dispersed liquid-droplet phase of the target material in the initial stage of irradiation by the neodymium laser is bulk vaporization (explosive vaporization) [1, 4, 24, 26, 27].

The authors of [26, 27] discussed various factors which facilitate bulk vaporization. These factors include space–time nonuniformity of the acting laser radiation, gases dissolved in the metal, and various inclusions and defects in the crystalline structure. Experiments conducted with targets obtained by powder metallurgical methods [31] confirm that the fine particles in the system are formed as a result of bulk vaporization. In these experiments, a neodymium-laser pulse with a duration of 10^{-3} sec and energies up to 1.5 kJ in the free-generation regime irradiated targets made of cold-rolled copper and copper made by powder metallurgical methods. The powder-based copper was made in two variants: pure, and with different amounts of a molybdenum addition. The diameter of the radiation spot on the target surface was 7.5 mm in each case. Probing with a ruby laser was done at a distance of 1.5 mm from the target surface. Figure 6 shows the results of the experiments in the form of the time dependence of the absorption and scattering coefficients for the probe radiation.

The dependences obtained for the rolled copper show that small particles of the target material (smaller than 0.7 μm) are present in the erosive jet at the beginning of disintegration. There is a change in the mechanism of particle formation by the end of the laser pulse and coarse particles enter the jet. An increase in the number of fine drops can be expected to be seen in porous metal due to the large gas content. This was confirmed by the curves illustrating the absorption and scattering of the radiation by products of the erosion of the copper target obtained by the powder metallurgical method. This material was considerably more porous than the cold-rolled copper (Fig. 6). In this case, absorption and scattering occur earlier than on the target of cold-rolled copper, while fewer coarse drops appear by the end of the pulse. It is apparent from the ratio of the scattering and absorption coefficients that, on the whole, the drops that are formed are more uniform during the entire period of radiation.

When radiation from the neodymium laser was directed onto a target made of copper with a 20% molybdenum addition (the copper having been obtained by powder metallurgical methods), particles of the target material were formed even earlier and absorption began to play an increasingly greater role in losses of the probe radiation. This indicates that the particles of the target material were present in the form of a finely dispersed phase. Such disintegration of the target material can be attributed to the fact that the molybdenum grains serve as boiling centers. Since molybdenum has a greater absorption coefficient than copper and a higher melting point, the molybdenum grains facilitate bulk vaporization. However, the same grains make it impossible for coarse drops to form. Thus, the ejection of the liquid melt characteristic of most metals is not seen by the end of the pulse. For a target with a molybdenum content of 50%, disintegration begins even earlier and the absorption coefficient is appreciably greater than the scattering coefficient. As a result, the particles are even smaller than in the previous case. For a target with a molybdenum content of 80%, the absorption of the probe radiation begins almost as soon as the pulse strikes the target, while significant scattering begins somewhat later and turns out to be less than absorption for the entire duration of the pulse. Thus, the particles of the target material are dispersed in the form of fine particles whose dimensions are at least considerably smaller than the wavelength of the radiation from the ruby laser (0.7 μm).

Photographs of the erosion zone after irradiation of the target offer qualitative proof of the above. Visible on the copper target are traces of splashed liquid formed by the hydrodynamic mechanism. In contrast, no such traces are seen in photographs taken of the target with 80% molybdenum.

Our experiments convincingly show that dissolved gases in metals and various inclusions facilitate bulk vaporization.

For example, when a zinc target (see Fig. 2) is acted upon by laser radiation, a finely dispersed liquid-droplet phase is formed from the very beginning of the pulse as a result of bulk vaporization. By the end of the pulse, there is a shift in the particle-formation mechanism and coarse particles appear in the erosive jet (these particles being formed by the hydrodynamic mechanism).

To determine the loss of laser radiation along an erosive jet, a jet formed from a zinc target was probed in the transverse direction at different distances h from the target surface [32, 33]. As was shown by the experiments in [32], the curves of the coefficients reach steady-state values for all probing heights after 50-100 μsec and change very little over the course of the next 500-600 μsec. Thus, the moment $t^* = 300$ μsec was chosen to reflect the fact that the absorption and scattering coefficients were steady at this moment in all of the experiments. The change in the steady values of the absorption coefficient K_{abs}^* and scattering coefficient K_{sca}^* was studied in relation to the probing height and the energy of the neodymium-laser radiation.

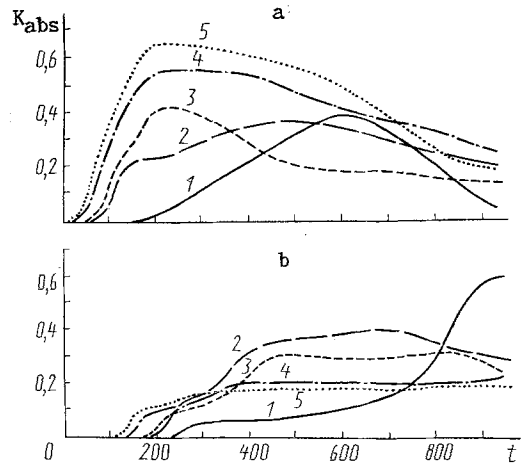

Fig. 6. Time dependence of the absorption coefficient (a) and scattering coefficient (b) for different targets: 1) cold-rolled copper; 2) copper made by powder metallurgy; 3, 4, 5) copper with 20, 50, and 80% additions of molybdenum.

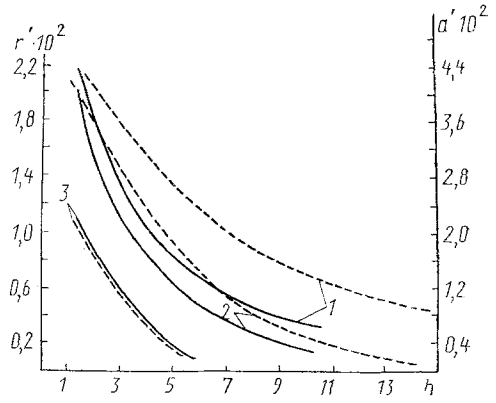

Fig. 7. Change in the absorption index (solid curves) and scattering index (dashed curves) along the jet with neodymium-laser energies of 1300 (1), 900 (2), and 340 J (3). r', cm^{-1}; a', cm^{-1}.

From the viewpoint of practical use, it is more important to know the absorption and scattering indices (which are independent of the dimensions of the medium being probed) than the absorption and scattering coefficients (which do depend on these dimensions). The indices were determined by using high-speed photographs of an erosive jet to determine the path over which probe radiation was scattered and absorbed [33]. The photographs were taken through an interference light filter with a transmission maximum at the generation wavelength of the probe laser (0.6943 μm).

Knowing the length of the path of interaction x of the probe radiation with the erosive jet for $t^* = 300$ μsec and the steady-state values of the absorption and scattering coefficients and using the conditions $K_{abs} = 1 - e^{a'x}$ and $K_{sca} = 1 - e^{-r'x}$, we find the natural absorption index a' and natural scattering index r'. Figure 7 shows measurements for different probing heights and different energies of the plasma-forming neodymium laser. The experiments showed that scattering and absorption decrease with height and, at h = 20 mm, could not be detected even at the maximum radiation power densities. Considering that x changes negligibly (~20%) in these experiments, we can attribute the decreases in a' and r' with increasing distance from the target to the complete vaporization of particles formed by bulk vaporization near the target surface as these particles move counter to the laser radiation. Since the difference between the wavelengths of the probe radiation from the ruby laser (~0.7 μm) and the plasma-forming radiation from the neodymium laser (~1 μm) was insignificant, it can be assumed that the erosive jet has the same shielding effect on the radiation from the plasma-forming laser as it does on the radiation from the probe laser.

Thus, part of the laser radiation is lost in the erosive jet and never reaches the target surface. Although this radiation is small for the erosive jet from a zinc target, it can have the effect of creating a denser medium than in the case of the adiabatic dispersal of transparent vapor by completing the vaporization of particles of the target material in the course of their motion counter to the laser beam. This residual vaporization in turn affects the threshold energy for the formation and propagation of shock waves, absorption spikes, etc.

However, these results apply only to the zinc target. It is very interesting to study the screening of radiation by particles from targets of other metals having different thermophysical characteristics. Theoretical estimates [2] and detailed unidimensional and two-dimensional calculations of a laser plasma with allowance for the condensed phase (particles entering the plasma from the target surface and particles formed by condensation of vapors as they expand while moving away from the surface) [7-10] show that the role of the condensate is very significant for a whole range of metals. This effect was studied in experiments [34] set up to probe an erosive jet by radiation from a ruby laser for targets of cadmium, lead, bismuth, magnesium, aluminum, copper, nickel, titanium, molybdenum, and tungsten. The materials of the targets were chosen so as to embrace a wide range of thermophysical parameters. Due to the probabilistic nature of neodymium-laser generation in the free regime and the transport of target material to the erosive jet, the coefficients $K_{tr}(t)$ and $K_{sca}(t)$ were averaged over several experiments. The jet was probed 1.5 mm from the target surface. The radiation of the plasma-forming neodymium laser was focused on the target surface in such a way that the focus of the lens was located behind the target and a spot 8 mm in diameter was illuminated on the surface. The energy of the radiation from the laser unit was regulated with neutral light filters so that the average power density on the target surface was 10^6 W/cm^2.

The results of the probing are shown in Fig. 8. According to this data, the metals that were studied can be conditionally divided into three groups. The first group contains metals with a relatively low boiling point (Cd, Pb, Zn, Bi, Mg), the second group contains metals with a moderate boiling point (Al, Cu, Ni), and the third group contains metals with a high boiling point (Ti, Mo, W). Metals with low melting and boiling points are characterized by the appearance of scattering at or just after the beginning of the radiation pulse from the neodymium laser (Fig. 8a-d). The scattering coefficient is negligible and changes little in the first half of the pulse, while in the second half it increases sharply and reaches its maximum value by the end of the radiation. The absorption coefficient is greater than the scattering coefficient at the beginning of the pulse but decreases in the second half of the latter.

Proceeding on the basis of Eqs. (3) and (4), it can be concluded that fine particles of the target material, i.e. particles of a diameter much smaller than the wavelength of the probe radiation, are formed at the beginning of the radiation pulse from the neodymium laser at the surface of targets made of cadmium, lead, bismuth, and magnesium – as in the case of zinc. The value of K_{sca} increases sharply and K_{abs} decreases by the end of the pulse (600-700 μsec), which is indicative of the predominance of coarse particles, i.e. particles with a diameter much greater than the wavelength of the ruby laser.

Thus, for low-melting metals, fine droplets of liquid are formed at the beginning of the pulse from the plasma-forming laser as a result of bulk vaporization. By the end of the pulse, this mechanism is replaced by the hydrodynamic mechanism of particle formation and fairly coarse drops appear in the erosive jet.

Somewhat more complicated is the behavior of K_{tr}, K_{abs}, and K_{sca} for magnesium (Fig. 8d). Insufficient energy reaches the surface due to the ejection of a large number of coarse particles, with the process beginning anew after the dispersal of these particles. This sequences of events was examined in detail in [34].

For metals with a higher boiling point (Al, Cu, Ni), there is a lag in the appearance of the scattering signal (Fig. 8e-g). For aluminum, appreciable scattering begins 300 μsec after the beginning of the pulse from the neodymium laser. The comparable times for copper and nickel are 500 μsec and 600 μsec. The time dependences of K_{tr}, K_{abs}, and K_{sca} for aluminum are qualitatively similar to the analogous curves for magnesium. This is further evidence of the intensive screening effect of coarse drops ejected into an area corresponding roughly to the middle of the pulse from the neodymium laser. At the beginning of the pulse, radiation losses are determined only by absorption on fine particles. For the copper target, the disintegration products have no effect on propagation of the radiation for the first 200 μsec. This fact is connected with the high reflection coefficient of copper for the laser radiation used in the experiment. Thus, the actual power density that goes into heating the target is considerably less than for the other metals that were studied. Fine drops begin to appear as a result of bulk vaporization only after the elapse of 200 μsec, while coarse drops are ejected by the end of the pulse. For the target made of nickel – which has higher melting and boiling points than copper – scattering on coarse drops begins even later, although absorption on fine drops plays an important role from the very beginning of the pulse.

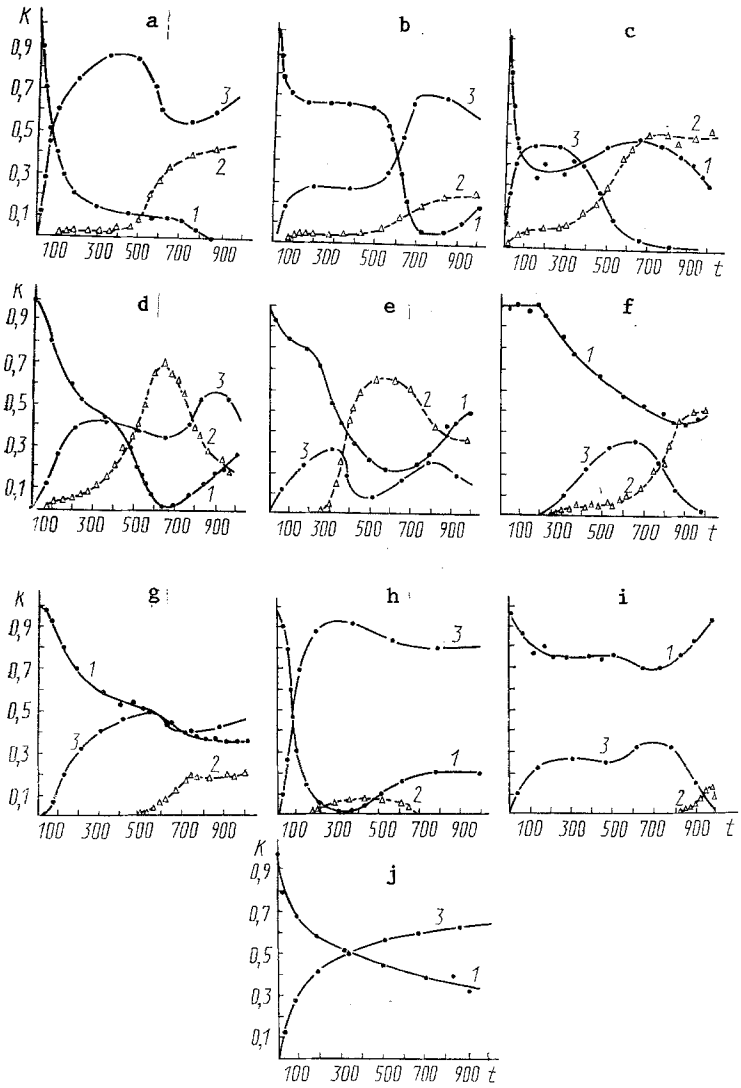

Fig. 8. Time dependences of the transmission coefficient (1), scattering coefficient (2), and absorption coefficient (3) for targets of cadmium (a), lead (b), bismuth (c), magnesium (d), aluminum (e), copper (f), nickel (g), titanium (h), molybdenum (i), and tungsten (j).

The effect of coarse particles on propagation of the laser radiation is negligible for metals with a very high boiling point (Ti, Mo, W) (Fig. 8h-j). Significant scattering on coarse particles occurs either by the end of the pulse (as in the case of molybdenum) or not at all (as in the case of tungsten). Absorption of the laser radiation due to the presence of small particles is very significant from the beginning of the pulse. This can be attributed to the fact that a relatively thin layer of liquid metal is formed by metals with a very high boiling point and a relatively low (compared to aluminum, for example) thermal conductivity. The thinness of the layer makes the ejection of coarse particles more difficult. It should be noted that absorption in the erosive jet of titanium can also occur as a result of resonance absorption at transitions lying within the generation region of the neodymium laser [35].

Thus, with a power density of 10^6 W/cm^2, the investigated metals are characterized by significant absorption of the laser radiation at the beginning of the pulse on a finely dispersed liquid-droplet phase formed by bulk vaporization. Over time, a fairly thick layer of molten metal is formed in the erosion crater as a result of heating by the laser radiation, radiation from the plasma jet, and the hydrodynamic mechanism. There is also a change in the mechanism by which particles of the target material are formed. The pressure pulse in the erosive jet ejects coarse drops from the crater, with appreciable absorption and scattering resulting in a significant loss of laser radiation on these drops. High-melting metals are exceptions to this. In this case, few or no coarse drops are ejected from the layer and the losses of laser radiation are determined mainly by absorption on small particles.

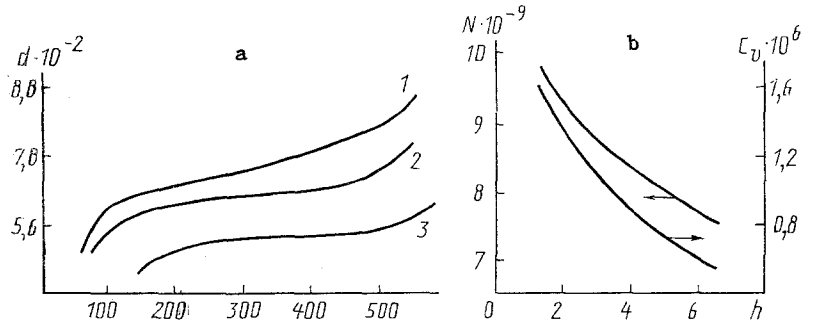

Fig. 9. Time dependence of the diameter of the liquid drops (a) and the change, along the jet, of the numerical N and volume C_v concentrations of liquid-phase particles (b) (1 – h = 1.5 mm; 2 – 3; 3 – 6). d, μm; N, cm^{-3}.

According to Eq. (3), the dimensions of the particles formed as a result of the mechanism of bulk vaporization are determined as $d << \lambda$. However, it is interesting to examine this question in greater detail. With this in mind, we used the empirical ratio of the scattering and absorption coefficients and the calculated dependence of this ratio on the diameter of the scattering particles to determine the dimensions of liquid drops of lead formed by bulk vaporization. The dimensions were determined in relation to the duration of the radiation pulse and probing height.

The scattering index σ_s and attenuation constant σ_a for optical radiation from the dispersion medium were determined theoretically by numerical integration of the corresponding monodisperse characteristics in accordance with the formulas

$$\sigma_a = \int_0^{d_f} k_a(d,\ n,\ \chi,\ \lambda)\frac{\pi}{4} d^2\varphi(d)\,\partial d \Big/ \int_0^{d_f} \frac{\pi}{6} d^3\varphi(d)\,\partial d,$$

$$\sigma_s = \int_0^{d_f} k_s(d,\ n,\ \chi,\ \lambda)\frac{\pi}{4} d^2\varphi(d)\,\partial d \Big/ \int_0^{d_f} \frac{\pi}{6} d^3\varphi(d)\,\partial d,$$

where d_f is the finite integration limit (the largest possible dimension of the scattering particles); $k_a(d, n, \chi, \lambda)$ is the attenuation efficiency factor, regarded as a function of the dimensions d, the real n and imaginary χ parts of the complex refractive index, and the wavelength of the radiation λ; $k_s(a, n, \chi, \lambda)$ is the scattering efficiency factor; $\varphi(d)$ is the particle-size distribution function. In our case, $\lambda = 0.69\ \mu$m, while the values n = 1.78 and $\chi = 3.57$ were determined experimentally for a lead melt by the ellipsometric method. The values of the efficiency factors were found on the basis of the Love–Mie theory [36]. The calculations were performed for the model of a polydisperse scattering medium characterized by a particle-size gamma distribution

$$\varphi(d) = \frac{C_v}{\Gamma(\mu+4)}\left(\frac{d}{d_0}\right)^{\mu+4}\exp\left(-\mu\frac{d}{d_0}\right),$$

where C_v is the volume concentration of scattering particles; d_0 is their most probable size; μ is the width parameter of the particle-size distribution; $\Gamma(x)$ is the gamma function of x.

We used the calculated values of scattering $\sigma_s(d)$ and absorption $\sigma_b(d)$ – the sum of which was equal to $\sigma_a(d)$ – to construct the theoretical dependence of the ratio of these coefficients σ_s/σ_b on particle diameter for different μ. Using the experimental ratio of $K_{sca}(t)$ and $K_{abs}(t)$ for lead and the theoretical curves of σ_s/σ_b, we constructed the dependences of the diameters of the liquid-phase particles on the duration of the pulse from the neodymium laser when the probing was done different distances h from the target surface (Fig. 9a).

The calculations showed that the curves for different μ nearly coincide at particle diameters less than 0.15 μm, although the curve with $\mu = 3$ corresponds to a polydisperse particle distribution and the curve with $\mu = 100$ corresponds in essence to a monodisperse distribution. Then the optical density created by the ensemble of particles attenuating the radiation $\tau = C_v\sigma_a l$, where l is the path over which the probe radiation undergoes scattering and absorption (l was determined experimentally from high-speed photographs obtained through a light filter with transmission in the region 0.69 μm [33]).

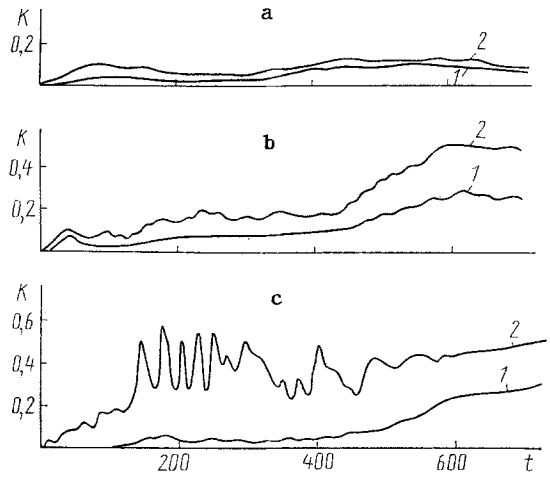

Fig. 10. Change in the scattering coefficient (1) and absorption coefficient (2) over time for a zinc target with a neodymium-laser energy of 350 (a), 730 (b), and 1550 J (c).

Having determined τ as the sum of the absorbed and scattered components, we can use the graphs of $K_{tr}(t)$ and $K_{sca}(t)$ to find the volume concentration of particles. Figure 9b shows the dependences of the volume C_v and numerical N particle concentrations on the distance to the target for the characteristic moment of time $t^* = 300$ μsec from the beginning of the pulse from the neodymium laser. The numerical concentration was found from the expression $C_v = NV_0$, where V_0 is the volume of a particle. This question was examined in greater detail in [37].

Thus, the completed experiments allowed us to determine the specific dimensions of particles of the liquid-droplet phase during their interaction with the laser radiation and the surrounding medium. The experiments showed that for all distances h from the target surface, an increase in the duration of the laser pulse is initially accompanied by a slow increase in drop diameter (100-400 μsec). Drop diameter then increases sharply, which is probably due to the transition from bulk vaporization to the hydrodynamic mechanism. For the same given moment of time, particle diameter decreases with an increase in h. This has to do with completion of vaporization of the liquid-droplet phase as it moves counter to the laser beam.

The above-described experiments were performed mainly with a radiation power density $\sim 10^6$ W/cm^2. Studies conducted at different power densities would have allowed us to determine the range within which particles of the liquid-droplet phase of the target material formed by bulk vaporization have a significant effect on the optical characteristics of the erosive jet. However, too much time would have been required to study the optical characteristics of the jet with broad variation of pulse energy for a number of different metals. An automatic system to record and analyze the relevant physical parameters has been developed for such investigations. This system – which makes it possible to record and store empirical data and perform all necessary computations in real time – is described in greater detail in [31, 38].

The experimental unit and method described in Fig. 1 were used together with the above-mentioned signal recording and analysis system to conduct studies at different power densities. The targets were plates of lead, cadmium, magnesium, bismuth, and zinc. The diameter of the irradiated spot on the target surface was 7.5 mm. The duration of the generation pulse from the neodymium laser was 0.9 msec. These values allowed us to easily find the power density of the radiation by knowing the energy in the pulse. Transverse probing of the erosive jet of the above-indicated metals for different energies of the plasma-forming neodymium laser showed that there is a threshold at which losses of probe-laser radiation become significant. The neodymium-laser power density at which this occurs depends on the thermophysical properties of the metal.

For a zinc target and a pulse energy of 320 J, the erosive products are transparent to the probe radiation for the entire duration of the main pulse. Only toward the end of the pulse do significant losses occur on erosion products in the form of coarse particles formed by the hydrodynamic mechanism. With an increase in the energy of the neodymium laser to 350 J, scattering and absorption of the probe radiation are seen from the very beginning of the pulse (see Fig. 10a). This fact is related to the formation of particles by bulk vaporization. With a further increase in the energy of the neodymium laser, losses of the probe radiation from the ruby laser increase as a result of both absorption and scattering. Figure 10b shows the time dependence of the absorption and scattering coefficients for an energy of 730 J. It is apparent that the scattering and absorption coefficients

change relatively smoothly over time. At neodymium-laser energies in excess of 1 kJ, spikes begin to appear on the absorption curve. With an increase in power density, the number of such transients increases with a relative increase in probe-radiation loss due to absorption. Meanwhile, the scattering coefficient even decreases somewhat in this case. Figure 10c shows the time dependence of the absorption and scattering coefficients for a neodymium-laser energy of 1550 J when a zinc target is irradiated. It can be seen from the figure that the absorption coefficient undergoes sharp fluctuations lasting about 40 μsec.

The authors of [39] recorded similar fluctuations of rebound pressure in the irradiation of a lead target by a neodymium laser in the free-generation and quasisteady regimes. In a study of the irradiation of aluminum alloy D16T by a neodymium laser in the quasisteady regime in [40], researchers observed fluctuations of scattered radiation of the plasma-forming laser and found a correlation between this scattering, the luminescence of the jet, and brightness temperature. However, the radiation of the laser was sharply focused on the target in these studies, resulting in the formation of a relatively deep crater. As a result, hydrodynamic processes occurring during the formation of the crater had a significant effect on the behavior of the erosion products. In our case, the diameter of the crater was 7.5 mm and its maximum depth after irradiation was only 0.3 mm. Thus, our results are difficult to compare with the results in [39, 40]. It should be noted that the pulse durations were very similar in [39, 40] and in Fig. 10c.

We conducted an additional experiment to explain this type of change in the absorption coefficient. Simultaneous with the probing of an erosive jet formed by the irradiation of a zinc target by a neodymium laser with an energy of 1320 J, we made spectroscopic measurements of the parameters of the plasma of the jet in the probe region with a time resolution of about 5 μsec. The same experiment was described in greater detail in [38]. Figure 11 shows time dependences of the temperature, electron concentration, and absorption index $\varkappa_{pl}$ of the plasma jet obtained by spectroscopic methods. Also shown is the absorption index of the erosive jet $\varkappa_e$ measured by the method of laser probing.

An analysis of the curves in Fig. 11 shows that plasma temperature and electron concentration increase along with the absorption index $\varkappa_{pl}$ when the absorption coefficient increases in the transversely probed erosive jet. It follows from this that there is a sudden increase in absorption in the plasma at the moment the absorption coefficient increases sharply (see Fig. 10c).

Comparison of the absorption indices of the plasma $\varkappa_{pl}$ and the erosive jet $\varkappa_e$ shows that not all of the absorption is governed by the plasma. Absorption in the erosive jet at the level $\varkappa_e \sim 0.15$ is recorded even when absorption in the plasma is negligible (see Fig. 11c and d), i.e. absorption occurs in the erosive jet in this case both as a result of the plasma and as a result of particles of the liquid-droplet phase. Additional proof of this comes from the presence of scattering of the probe radiation on the jet.

The following pattern can be discerned on the basis of the above. At pulse energies lower than 320 J, products of the disintegration of the zinc target enter the erosive jet in the form of transparent vapors. With an increase in power density, liquid drops appear at the very beginning of the pulse due to bulk vaporization, and absorption and scattering of the probe radiation from the ruby laser become significant.

With a further increase in the power density of the neodymium-laser radiation, the number of particles of the target material increases. This in turn leads to an increase in absorption and scattering on these particles. Moving in the radiation field of the neodymium laser, the liquid-droplet particles absorb this radiation and, vaporizing, create a denser medium. This in turn allows absorption to proceed more intensively. Sudden increases in absorption occurred with a sharp increase in the parameters (T, N_e, and $\varkappa_{pl}$) of the plasma in our experiments with a zinc target when the energy reached 1050 J. This increase in absorption occurred on a denser medium formed by certain particles. It should be noted that not all of the particles were completely vaporized in this instance. An analysis of the behavior of the absorption and scattering coefficients shows that only 1-3 absorption spikes – each lasting about 40 μsec – appear during the laser pulse at this power density. For the remainder of the pulse, absorption and scattering in the erosive jet are determined by the particles. It is only with a further increase in the energy of the neodymium laser that the spikes become nearly regular and absorption begins to be determined mainly by the plasma (see Fig. 10c). The fraction of probe radiation that is scattered in this case decreases, which can be attributed to a decrease in particle size and concentration.

A detailed analysis of the results of experiments involving probing with the use of computers showed that many (but not all) of the spikes appear when the amplitude of the beam generated by the neodymium laser is 2-3 times greater than the mean amplitude.

With a further increase in the power density of the neodymium-laser radiation, particles located 1.5 mm from the target surface may be completely vaporized and the scattering coefficient for the probe radiation may decrease to zero. Studies of the erosive jets of other metals showed qualitatively similar results. This subject was examined in greater detail in [38].

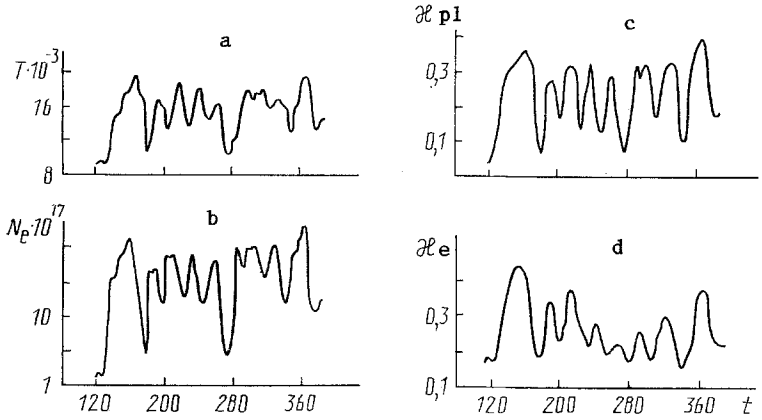

Fig. 11. Time dependences of temperature (a), electron concentration (b), and the absorption indices of the plasma (c) and erosive jet (d) for a zinc target with a plasma-forming-laser energy of 1320 J. $\varkappa_{pl}$, $\varkappa_e$ cm^{-1}.

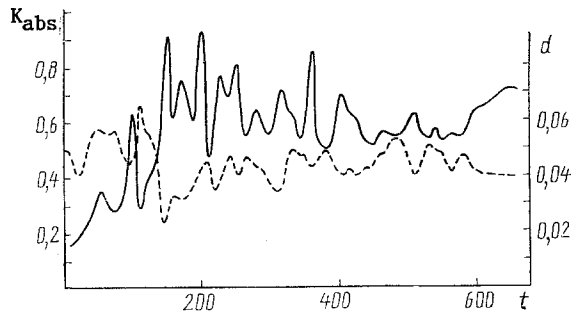

Fig. 12. Change over time in the absorption coefficient (solid curve) and particle diameter (dashed curve) in the erosive jet of a nickel target with a power density of 4.8 MW/cm^2 for the plasma-forming laser. d, μm.

Experiments conducted in [41] used the above-described methods to simultaneously monitor the absorption coefficient in the erosive jet and the diameter of the target-material particles. The results showed that particle diameter decreases when the absorption coefficient increases. This confirms that the mechanism of low-threshold breakdown (absorption bursts) is operative in the erosive jet due to complete particle vaporization. Figure 12 shows results of an individual experiment involving the irradiation of a nickel target by a neodymium laser with a power density of $4.8 \cdot 10^6$ W/cm^2. It is apparent that numerous absorption bursts occur in the erosive jet as particle diameter decreases.

Experiments conducted in [41] with a neodymium laser operated at different energies showed that particle size decreases with an increase in the power density of the plasma-forming radiation and the particles appear earlier in the erosive jet. This can be attributed to the fact that heating of the molten metal occurs more intensively within a thinner layer with an increase in power density in the radiation zone. As a result, finer particles enter the erosive jet due to bulk vaporization. Moving counter to the laser beam, the particles are rapidly vaporized and, upon entering the probe region (h = 1.5 mm), may be of even smaller dimensions (see Fig. 13).

One more piece of evidence in support of complete vaporization of the liquid-droplet phase as it moves counter to the laser beam is data from experiments which studied erosive laser jets from a copper target by means of a multichannel optical spectrum analyzer [42]. Figure 14 shows changes in pressure P and density ρ found by spectroscopic methods along the erosive jet of a copper target irradiated by a neodymium laser with an energy of 1.5 kJ. The duration of the pulse was 10^{-3} sec. The diameter of the irradiated spot was 7.5 mm. The curves shown in the figure correspond to a moment (600 μsec) when the erosive jet had already formed and was in the steady state. It is apparent from Fig. 14 that pressure increases at distances up to 10–12 mm. It then decreases with increasing distance from the target surface due to gasdynamic dispersal. It increases again at a distance of 30 mm in the normal shock wave associated with the underexpanded supersonic plasma jet [1, 3]. The path of the

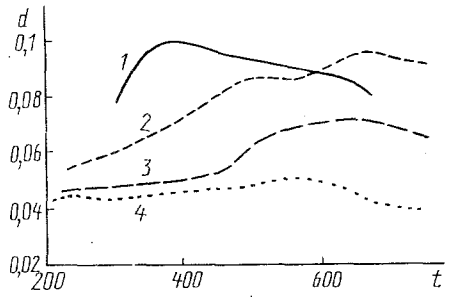

Fig. 13. Change over time in the dimensions of particles in the erosive jet of a nickel target at neodymium-laser power densities of 1.6 (1), 2 (2), 2.5 (3), and 3.3 MW/cm^2 (4).

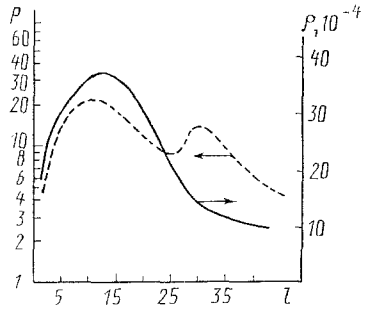

Fig. 14. Change in the pressure P and density ρ of vapors along the erosive jet of a target at the moment of time t* = 600 μsec. P, atm; p, g/cm^3.

density curve along the jet indicates that pressure increases on the initial section not only due to an increase in temperature, but also due to the entry of additional vapor into the jet. This can be explained only by residual vaporization of particles of the liquid-droplet phase. Experiments involving laser probing also showed that particles of this phase are almost completely vaporized at distances of 10–12 mm from the target surface.

Thus, studies of the optical characteristics of the erosive jets of metals have shown that particles formed as a result of bulk vaporization enter a jet which initially consists of transparent vapors when the intensity of the acting radiation is increased. These particles then scatter and absorb the laser radiation. Moving counter to the laser beam and vaporizing, they create around themselves a medium which is denser than that which results from the adiabatic dispersal of the vapors. When a certain value of power density characteristic of each metal is reached, some of the particles initiate bursts in the surrounding medium; the number of such bursts subsequently increases to the point where the particles are nearly completely vaporized.

Experiments conducted with a large group of metals made it possible to determine the dynamic range of neodymium laser free-regime power densities in which the particles formed from the targets of each metal by bulk vaporization exert a significant effect on the optical characteristics of the erosive laser jet. When the power density of the radiation is below this range, the erosive products that are formed are transparent to the radiation. This case was examined theoretically in [2]. When the range is exceeded, radiation losses are determined mainly by absorption in the plasma. Plasma breakdown or absorption transience was studied in detail theoretically in [43, 44]. These ranges are as follows for the above-investigated metals (MW/cm^2): zinc – 0.9-2.65, lead – 0.3-0.9; cadmium – 0.7-1.9; magnesium – 0.7-2.2; bismuth – 0.25-2.15; aluminum – 1.3-3.0; nickel – 1.6-3.3; copper – 4.0-12.0; titanium – 0.7-1.1; tungsten – 2.6-4.2; zirconium – 2.6-5.6; molybdenum – 1.7-4.8.

The results of these studies need to be taken into account both in theoretical models and in actual interactions of laser radiation with metals, in order to optimize processing regimes.

LITERATURE CITED

1. L. Ya. Min'ko, Generation and Study of Impulsive Plasma Flows [in Russian], Minsk (1970).
2. S. I. Anisimov, Ya. A. Imas, G. S. Romanov, and Yu. V. Khodyko, Action of High-Intensity Radiation on Metal [in Russian], Moscow (1970).
3. M. A. El'yashevich, V. K. Goncharov, L. Ya. Min'ko, and G. S. Romanov, Zh. Prikl. Spekstrosk., **15**, 200-204 (1971).
4. V. K. Goncharov, L. Ya. Min'ko, S. A. Mikhonov, and V. S. Strizhnev, Kvantovaya Élektron., No. 5, 112-116 (1971).
5. V. K. Goncharov, L. Ya. Min'ko, S. A. Mikhnov, and V. S. Strizhnev, ibid., No. 1 (13), 56-62 (1973).
6. L. Ya. Min'ko and A. N. Chumakov, Zh. Prikl. Spekstrosk., **27**, 999-1003 (1977).
7. I. M. Kozlov, G. S. Romanov, and A. V. Teterev, "Effect of particles of a condensed phase on the parameters of erosive light beams," Submitted to VINITI, Reg. No. 1972-82. Minsk (1982).
8. I. M. Kozlov, G. S. Romanov, Yu. A. Stankevich, and A.V. Teterev, Summary of Documents of the VI All-Union Conference on the Non-Resonance Interaction of Light Radiation with Substances. Vilnius, 1984, pp. 284-285.
9. I. M. Kozlov, G. S. Romanov, Yu. A. Stankevich, and A. V. Teterev, Mathematical Models and Analytical and Numerical Methods in Transport Theory [in Russian], Minsk (1986).
10. V. K. Goncharov, V. I. Karaban , and A. V. Kolesnik, Kvantovaya Élektron., **12**, 762-766 (1985).
11. V. I. Goncharov, V. I. Karaban', and A. V. Kolesnik, Kvantovaya Élektron., **12**, 762-766 (1985).
12. G. Grim, Plasma Spectroscopy [Russian translation], Moscow (1969).
13. A. Burges and M. Seaton, Mon. Not. R. Astron. Soc., **120**, No. 2, 121-151 (1960).
14. W. Karzas and R. Latter, Astrophys. J. Suppl. Ser., No. 6, 167-172 (1961).
15. D. Inglis and E. Teller, Astrophys. J., No. 90, 439-443 (1939).
16. Optical Properties of Hot Air [in Russian], Moscow (1970).
17. V. A. Kas'yanov and A. N. Starostin, Zh. Éksp. Teor. Fiz., **48**, 295-302 (1965).
18. Ya. B. Zeldovich and Yu. P. Raizer, Physics of Shock Waves and High-Temperature Gasdynamic Phenomena [in Russian], Moscow (1966).
19. V. Lokhte-Khol'tgreven (ed.), Methods of Studying Plasmas, Moscow (1971).
20. A. P. Burmakov and A. G. Shashkov, Properties of a Low-Temperature Plasma and Methods of Diagnosing It [in Russian], Novosibirsk (1977).
21. V. M. Ginzburg and Yu. I. Filenko, Zh. Tekh. Fiz., **40**, 2217-2220 (1970).
22. P. I. Ulyakov, Zh. Éksp. Teor. Fiz., **52**, 820-830 (1967).
23. O. I. Putrenko and A. A. Yankovskii, Zh. Prikl. Spektrosk., **15**, 596-604 (1971).
24. N. N. Rykalin, A. A. Uglov, and A. N. Kokora, Laser Treatment of Materials [in Russian], Moscow (1975).
25. Yu. V. Afanas'ev and O. N. Krokhin, Tr. Fiz. Inst. Akad. Nauk SSSR, Kvantovaya Radiofiz., **52**, 118-170 (1970).
26. B. M. Zhiryakov, N. N. Rykalin, A. A. Uglov, and A. K. Finnabo, Zh. Tekh. Fiz., **41**, 1037-1042 (1971).
27. N. N. Rykalin and A. A. Uglov, Fiz. Khim. Obrab. Mater., No. 2, 30-33 (1970).
28. V. K. Goncharov, V. I. Karaban', A. V. Kolesnik, and V.A. Lozhkin, Kvantovaya Élektron., **11**, 784-789 (1984).
29. G. Van de Hulst, Light-Scattering by Small Particles [Russian translation], Moscow (1961).
30. A. G. Bloch, Principles of Radiative Heat Transfer [Russian translation], Moscow, Leningrad (1962).
31. V. N. Barinov, A. P. Byk, V. K. Goncharov, et al., "Automated system to study time-dependent processes in the interaction of moderate-intensity laser radiation with a material," Preprint, Institute of Physics of the Academy of Sciences, No. 38, Moscow (1986).
32. V. K. Goncharov, V. I. Karaban', and A. V. Kol'esnik, Zh. Prikl. Spektrosk., **43**, 389-395 (1985).
33. V. K. Goncharov and V. I. Karaban', ibid., **45**, 22-25 (1986).
34. V. K. Goncharov, V. I. Karaban', and V. A. Ostrometskii, Kvantovaya Élektron., **13**, 1235-1240 (1986)
35. V. F. Loskutov and P. I. Ulyakov, Pis'ma Zh. Tekh. Fiz., No. 6, 336-339 (1978).
36. K. S. Shif'rin, Light-Scattering in a Turbid Medium [in Russian], Moscow (1961).
37. V. K. Goncharov, V. I. Karaban', A. V. Kol'esnik, and I. M. Radyuk, Kvantovaya Élektron., **15**, 2575-2577 (1988).
38. A. P. Byk, V. K. Goncharov, V. V. Zakhozhii, et al., ibid., **15**, 2552-2559 (1988).
39. B. M. Zhiryakov, N. I. Popov, and A. A. Samokhin, Zh. Éksp. Teor. Fiz., **75**, 494-503 (1978).
40. L. Ya. Min'ko, A. N. Loparev, V. I. Nasonov, and A. M. Kovalev, Kvantovaya Élektron., **12**, 1211-1219 (1985).
41. A. P. Byk, V. K. Goncharov, V. I. Karaban', and A. F. Chernyavskii, Kvantovaya Élektron., **16**, 1042-1046 (1989).

42. V. K. Goncharov, V. I. Karaban', A. V. Kolesnik, et al., Zh. Prikl. Spektrosk., **51**, No. 1, 16-22 (1989).
43. G. G. Vilenskaya and I. V. Nemchinov, Zh. Prikl. Mekh. Tekh. Fiz., No. 6, 3-19 (1969).
44. G. G. Vilenskaya and I. V. Nemchinov, Dokl. Akad. Nauk SSSR, **186**, 1048-1051 (1969).

PHYSICAL ESSENCE OF EROSIONAL PLASMA FORMATION AND THE FORMATION OF PLASMA FLOWS BY THE ACTION OF DIFFERENT TYPES OF HIGH-ENERGY SOURCES ON ABSORBING CONDENSED MEDIA

L. Ya. Min'ko

UDC 539.95

A study is made of erosional plasma processes occurring with the exposure of metals to a laser beam, a plasma, and a combination of the two. It is found that the ionization of the initially heated vapors is of a thermal nature, whether an erosional plasma is formed by an impulsive electrical discharge or a near-surface optical discharge.

Different types of energy sources – electrical discharges, plasma discharges, laser beams, and beams of electrons and ions – are used to obtain low-temperature plasmas. Practical applications of these energy sources for the welding, cutting, and heat treatment of materials shows that the physical processes involved in the high-energy loading of materials have much in common with one another. This commonality is based foremost on the similarity of the thermophysical processes that take place when absorbing condensed media are acted upon by different types of high-energy sources within the power-density range 10^5-10^7 W/cm^2. Evidence of this comes from the effective use of classical thermophysical representations [1] in descriptions of the above-mentioned manufacturing processes [2]. The subsequent refinement of these concepts for the high-energy loading of materials by different types of sources led to the discovery of a universal mechanism entailing oscillation of the surface temperature of the material [3]. When high-energy sources with a power density 10^3-10^7 W/cm^2 which remains constant over time act on the interface between the gaseous medium and the material, a heat flux which is variable over time may be created in the material. This heat flux is due to the screening of the material from the energy associated with near-surface gases or plasma by the flow of atoms (in the case of vaporization of the material) or electrons (in the case of thermionic emission) from the material's surface. The conclusion that the mechanism of oscillation of the surface temperature of the material and the density of the near-surface gas or plasma medium is universal is based on the following fact. For high-intensity loading involving different sources and different materials, there are certain vaporization or thermionic emission regimes which are governed by the same gasdynamic or plasmodynamic laws and in which the gas or plasma medium that is formed has the same surface-screening effect. This effect amounts to a reduction in the energy flux reaching the surface of the material. The above-described oscillation mechanism can, in conjunction with stability theory and the theory of nonlinear oscillations, be used to explain a large number of empirical phenomena that were previously not fully understood. These phenomena include pulsative vaporization, periodic explosive vaporization, and fusion and vaporization instability. The mechanism can also help explain the pulsating, nonmontonic time dependences of the physical quantities that characterize the loading process.

Detailed studies have been made of erosional plasma processes in the treatment of metals by laser beams, plasmas, and combinations of the two. Previous representations on the characteristics that plasma formation by the optico- and electroerosive mechanisms have in common [4] have been refined by using analogies between the physical processes which take place during electrical discharges and laser irradiation [5]. It was shown that erosional plasma formation in an impulsive electric discharge is

Institute of Physics, Academy of Sciences of Belarus, Minsk. Translated from Inzhenerno-Fizicheskii Zhurnal, Vol. 62, No. 5, pp. 685-686, May, 1992. Original article submitted December 16, 1991.

1062-0125/92/6205-0487$12.50